Enantioselective Recognition of Chiral Guests by the Water-Soluble Chiral [Mo$_{132}$O$_{372}$(H$_2$O)$_{72}$(x-Lactate)$_{30}$]$^{42-}$ Nanocapsules

Nancy Watfa, Weimin Xuan, Zoë Sinclair, Robert Pow, Yousef M. Abul-Haija, De-Liang Long and Leroy Cronin*

School of Chemistry, University of Glasgow, Glasgow G12 8QQ, UK

Supporting Information Placeholder

ABSTRACT: Investigations of chiral host guest chemistry are important to explore recognition in confined environments. Here, by synthesizing water-soluble chiral porous nanocapsule based on the inorganic metal-oxo Keplerate-type cluster, {Mo$_{132}$} with chiral lactate ligands with the composition [Mo$_{132}$O$_{372}$(H$_2$O)$_{72}$(x-Lactate)$_{30}$]$^{42-}$ (x = D or L), it was possible to study the interaction with a chiral guest, L/D-carnitine and (R/S)-2-butanol in aqueous solution. The enantioselective recognition was studied by quantitative ^{1}H NMR and ^{1}H DOSY NMR which highlighted that the chiral recognition is regulated by two distinct sites. Differences in the association constants (K) of L- and D-carnitine, which, due to their charge, are generally restricted from entering the interior of the host, are observed, indicating that their recognition predominantly occurs at the surface pores of the structure. Conversely, a larger difference in association constants (K$_S$/K$_R$ = 3) is observed for recognition within the capsule interior of (R)- and (S)-2-butanol.

Chiral recognition has been explored by designing artificial hosts including cyclodextrins,[1] calixarenes,[2] cucurbiturils,[3,4] crown ethers,[4] and chiral cages.[5] Despite the development of chiral organic and metal-organic hosts, the use of inorganic hosts is limited. This is due to the difficulty of producing chiral inorganic compounds, and their inherently weak interactions with chiral organic guests. Polyoxometalates (POMs) are unique hosts for enantioselective discrimination. This is because chiral POMs can be obtained by breaking the local symmetry of the clusters[6] or through chiral induction from chiral building blocks,[7] but discrimination of racemic guests by chiral porous POM hosts has not yet been reported.

Recently, we demonstrated that the stereoselective synthesis of chiral, gigantic Mo Blue clusters combining the approaches of symmetry-breaking and chiral induction.[8] This encouraged us to chirally functionalize another molybdenum-based cluster – the porous {Mo$_{132}$} Keplerate-type structure.[9] This cluster has a general formula of [{(Mo)Mo$_5$}$_{12}${Mo$_2$}$_{30}$]$^{42-}$ and can be regarded as a high-symmetry, spherical capsule constructed of 12 {(Mo)Mo$_5$} pentagonal-type units and 30 {Mo$_2$} linker-type units. The presence of 20 hexagonal Mo$_9$O$_9$ pores on the outer surface allow access to the inner cavity, which has an approximate volume of around 700 Å^3. The {Mo$_2$} linkers are weakly coordinated by bidentate ligands such as sulfate and acetate, which can be easily replaced by other carboxylate ligands, thus allowing the facile modification of the interior properties of the capsule such as charge density and hydrophobicity.[10] Due to its solubility in water and an accessible interior cavity, the anionic {Mo$_{132}$} capsule has been used as a host to interact with different cationic guests including tetramethylammonium,[11] guanidinium[12] and protonated urea.[13] Also, hydrophobic neutral guests such as benzene and alkanes have been encapsulated

within its hydrophobic cavity when functionalized by acetate and propionate.[14] However, this capsule has not been explored for enantioselective recognition of chiral guests. Therefore, functionalization of {Mo$_{132}$} with chiral carboxylate ligands that can provide a confined chiral interior space and surface pores that are accessible for enantioselective recognition of chiral guests will expand the scope of this capsule in asymmetric catalysis, chiral sensing and chiral separation (Scheme 1).
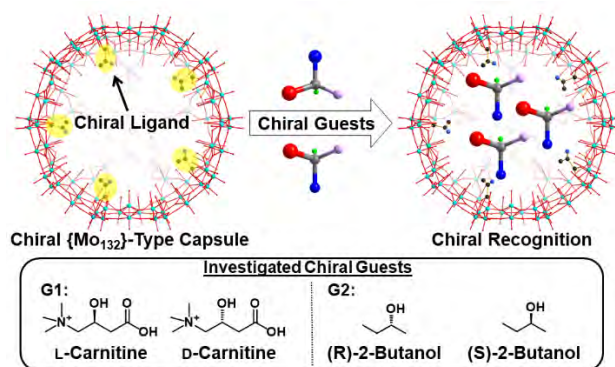
Scheme 1. Representation of chiral recognition within {Mo$_{132}$}, bearing chiral lactic acid as an interior ligand. Mo – turquoise, O – red, carbon – dark grey.

Herein, we describe the synthesis of two chiral {Mo$_{132}$} capsules (NH$_4$)$_{49}$[Mo$_{132}$O$_{372}$(H$_2$O)$_{72}$(L-C$_3$H$_5$O$_3$)$_{30}$](C$_3$H$_5$O$_3$)$_5$(SO$_4$) (H$_2$O)$_{200}$ **(L-1)** and (NH$_4$)$_{46}$[Mo$_{132}$O$_{372}$(H$_2$O)$_{72}$(D-C$_3$H$_5$O$_3$)$_{30}$] (SO$_4$)$_2$(H$_2$O)$_{250}$ **(D-1)**, using L- or D-lactate as chiral ligands and demonstrate their chiral recognition towards L/D-carnitine and (R)/(S)-2-butanol in aqueous solution. The two enantiomeric compounds **L-1** and **D-1** were fully characterized by single crystal X-ray diffraction, ^{1}H NMR, ^{13}C NMR, as well as circular dichroism (CD), and the formulae were established based on elemental analysis, FTIR and TGA (refer to SI). The capsules synthesized **L-1** and **D-1** exhibited enantioselective recognition towards L/D-carnitine and (R)/(S)-2-butanol owing to the selective interaction of these guests by surface pores and the interior cavity, respectively, as demonstrated by detailed ^{1}H NMR study. To the best of our knowledge, this is the first example of chiral recognition achieved by porous POM capsules in aqueous solution. The enantiomerically pure **L-1** and **D-1** were synthesized by adding 220 equivalents of the sodium salt of L- or D-lactate into an aqueous solution of {Mo$_{132}$(SO$_4$)},[15] respectively. Upon ligand exchange of sulfate with lactate, single crystals suitable for X-ray crystallographic analysis were harvested after slow evaporation. Single crystal X-ray structure analysis of **L-1** reveals the typical spherical {Mo$_{132}$} capsule functionalized with L-lactate. The molybdate framework can be regarded as an icosahedron in

which the twelve $\{(Mo^{VI}) Mo^{VI}_5O_{21}(H_2O)_6\}$ pentagonal units are placed at the vertices of the icosahedron and linked by the 30 $\{Mo_2^VO_4\}^{2+}$ dinuclear linkers.
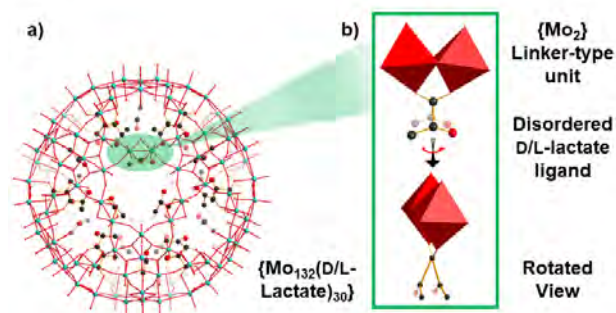
Figure 1. a) Ball-and-stick representation of **L-1** showing the co-ordinated L-lactate ligands. **b)** Perpendicular representations of the linking mode of the coordinated ligand to $\{Mo_2^V\}$ linker where the carbon chains are disordered over two positions (Figure 1). Mo – turquoise, O – red, carbon – dark grey.

The L-lactate ligands coordinate to the $\{Mo_2^VO_4\}^{2+}$ linkers *via* their carboxylate functional group, which are unambiguously assigned, while the atoms of the ligand tail are disordered over two positions (Figure 1). **D-1** is isostructural to **L-1** but functionalized by D-lactate. Despite the use of enantiopure L- and D-lactate during the self-assembly, their absolute chiral configuration could not be fully identified in the crystal structure and, as a result, both **L-1** and **D-1** crystallize in the R-3 centrosymmetric space group, rather than a chiral space group. This is caused by the high symmetry of the $\{Mo_{132}\}$ framework (I_h), which dominates the overall symmetries of **L-1** and **D-1**
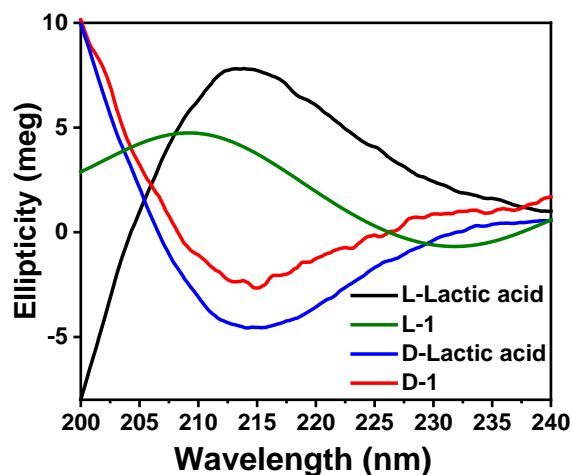
**Figure 2.** CD spectra of **L-1** and **D-1** compared to L-lactic acid and D-lactic acid in H_2O.

Although **L-1** and **D-1** cannot manifest their chirality in the solid-state, the presence of L-lactate or D-lactate leads to the CD response of **L-1** and **D-1** in solution, which are mirror images of each other, thus demonstrating their differing optical activities as a result of their chiral nature. The solution CD spectra of **L-1** and **D-1** exhibit a peak centered at 214 nm that originates from the lactate ligands (Figure 2). Compared with free lactate, there are only slight differences in the CD signals, indicating the chirality of lactate is preserved upon coordination to $\{Mo_{132}\}$. The CD signal corresponding to $\{Mo_{132}\}$ is, however, not detected in the long wavelength area

due to the rather strong adsorption arising from intervalence charge-transfer between Mo^V and Mo^{VI} centers in $\{Mo_{132}\}$, which greatly suppresses the CD response transferred by lactate ligands. The same phenomenon has also been observed in chiral Mo Blue clusters where the CD signal is not seen for the parent framework.

The ^{1}H NMR (Figure S6) and ^{13}C NMR (Figure S5) of compound **L-1** show two sets of well-resolved signals corresponding to free L-lactate and encapsulated L-lactate ligands. The broad signals belong to encapsulated ligands and are found upfield (2.9 ppm and 0.1 ppm, respectively) with respect to the corresponding sharp signals of the free lactate species. This assignment was supported by ^{1}H DOSY NMR where the diffusion coefficient of the L-lactate decreased from 5.20×10^{-10} m^2/s for the solvated molecules to 1.11×10^{-10} m^2/s for the molecules encapsulated within $\{Mo_{132}\}$ (Figure 3). The presence of both encapsulated and free, solvated lactates demonstrates that $\{Mo_{132}\}$ is still intact in the solution and the lactates are well aligned inside the cavity, available as chiral centers for enantioselective recognition. Also, the UV-vis-NIR spectra of **L-1** and **D-1** show the characteristic adsorption bands as $\{Mo_{132}\}$-acetate, further confirming their stability in solution (Figure S2).
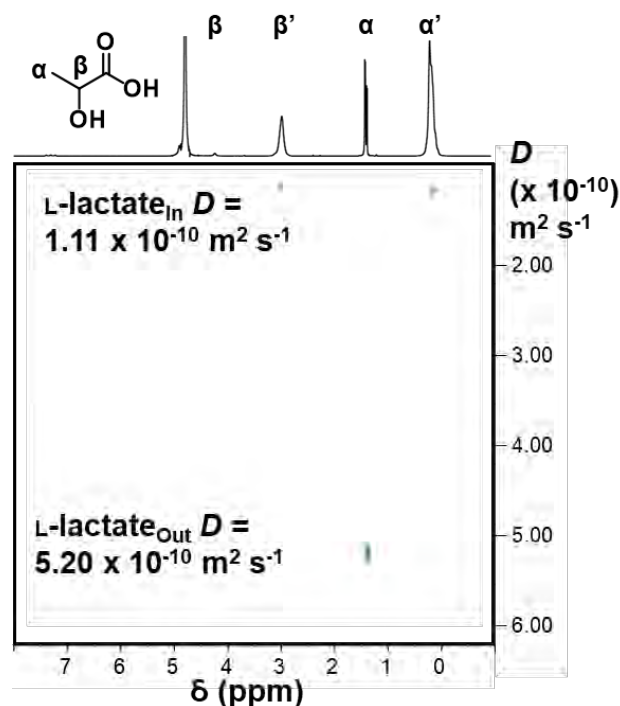

Figure 3. ^{1}H DOSY NMR spectrum of **L-1** (3 mM, 600 MHz, D$_2$O, 25 °C), highlighting the free and encapsulated L-lactate signals.

After confirming the chirality and stability of **L-1** and **D-1** in solution, we examined their chiral recognition of chiral guests. To do so, different guests were chosen to determine the enantioselectivities based on the two potential recognition sites (surface pores and inner cavity) of the host using ^{1}H NMR and ^{1}H DOSY NMR spectroscopy. We first tested the interactions between **L-1** and **D-1** and L/D-carnitine (abbreviated as L-G1 and D-G1, Scheme 1), which are expected to exclusively interact with the surface pores as guests bearing a quaternary ammonium group. This preferred affinity to the surface pores has been previously shown by Cadot *et al.*[11b] Introducing 5 equivalents of L-G1 or D-G1 to a 5 mM D$_2$O solution of **L-1** led to an obvious downfield shift in the NMR signals of carnitine (Figure S10), suggesting that L-G1 or D-G1 is bound to the surface pores of **L-1**, in a fast exchange on the NMR timescale.

However, the Δδ value was higher with D-G1 (Δδ = 0.25 ppm) than that of L-G1 (Δδ = 0.22 ppm), implying that **L-1** shows a preference of binding to D-G1. This observation was also supported by ^{1}H DOSY NMR where the diffusion coefficient of D-G1 dropped from 8.0 x 10^{-10} m[2]/s to 2.7 x 10^{-10} m[2]/s in the presence of **L-1** while this value decreased to 3.2 x 10^{-10} m[2]/s for L-G1. In contrast to the sole affinity of the quaternary ammonium group to the surface pores of $\{Mo_{132}\}$, as previously discussed, the ^{1}H NMR spectrum displayed an additional broadened peak at approximately 2.1 ppm, which is related to the interaction of the methyl-ammonium groups of the carnitine with the $\{Mo_{132}\}$ structure, in a slow exchange mechanism on the NMR timescale. This peak assignment has been confirmed with phase-sensitive Heteronuclear Single-Quantum Correlation (HSQC) NMR experiments (Figure S11) and indicates that a small amount of carnitine enters the capsule interior.

To quantify the different interactions between L-G1 and D-G1 with the pores of **L-1**, the association constants were calculated by the variation of diffusion coefficient of NMe_3^+ of L-G1 and D-G1 as a function of concentration of **L-1** (Figure 4). The association constant for L-G1 • **L-1** was found to be 950 ± 0.6 M^{-1} and that of D-G1 • **L-1** was 1300 ± 0.8 M^{-1}, thus demonstrating the selectivity of **L-1** towards D-G1. It should be noted that in the presence of another enantiomer **D-1**, the opposite trend is observed for L-G1 and D-G1. The relatively indistinct discrimination between L-G1 and D-G1 by the chiral hosts is probably caused by the inability of the introduced guests to directly interact with the chiral lactate ligands as they are not immediately proximal to the chiral centers, therefore weak chiral recognition with guests is expected.
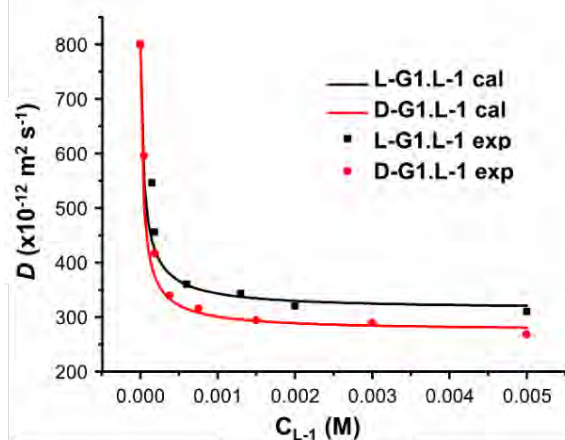

Figure 4. Variation of self-diffusion coefficients (D) for NMe_3^+ of L-G1 (black squares) and D-G1 (red circles) in presence of different concentrations of **L-1**. Black and red lines correspond to calculated diffusion coefficients.

To increase the enantioselective behavior of the host, we next explored the chiral recognition that occurs within the **L-1** cavity using a smaller compound, 2-butanol, which should be able to diffuse freely through the surface pores and access to the lactates inside the cavity. Upon addition of 300 equivalents of (R)-2-butanol, ((R)-G2), or (S)-2-butanol, ((S)-G2), to the aqueous solution of **L-1** (50 mg, D₂O) at 70 °C for 24 h, the formation of a stable host-guest complex is observed by ^{1}H NMR spectroscopy (Figure 5). The ^{1}H NMR spectra show the presence of new signals attributed to encapsulated (R)-G2 signals with upfield shift of Δδ = 0.7 ppm relative to that of the free guest (Figure 5).

These observations suggest binding between (R)-G2 and **L-1** is slow on NMR timescale and the upfield shift is caused by the shielding effect of **1**, thereby suggesting (R)-G2 is encapsulated

inside the $\{Mo_{132}\}$ rather than the surface pores. The broad NMR signals of (R)-G2 • **L-1** could either be derived from an intermediate rate of exchange between free and bound guests on the NMR timescale, or the reduced freedom of (R)-G2 guests caused by the restricted motion within the capsule cavity. The host-guest complexation is probably derived from multiple non-covalent interactions such as hydrogen bonding between lactate hydroxyl groups and the hydroxyl groups on (R)-G2 as well as the van der Waals forces between the hydrophobic side chains of lactate and (R)-G2.

When (S)-G2 is added, the newly formed signals were well resolved and showed an upfield shift of Δδ = 1 ppm relative to those of free (S)-G2. Compared with (R)-G2, these peaks were much more intense and had a greater upfield shift of ~ 0.3 ppm. The spectrum of racemic G2 (Rac-G2) is an intermediate between (S)-G2 and (R)-G2, with both the intensities and chemical shifts of the NMR signals falling between the related peaks corresponding to (S)-G2 and (R)-G2 (Figure 5: dashed box). These results suggest that **L-1** interacts preferentially with (S)-G2, thus allowing a stronger binding with (S)-G2 and selective adsorption of (S)-G2.
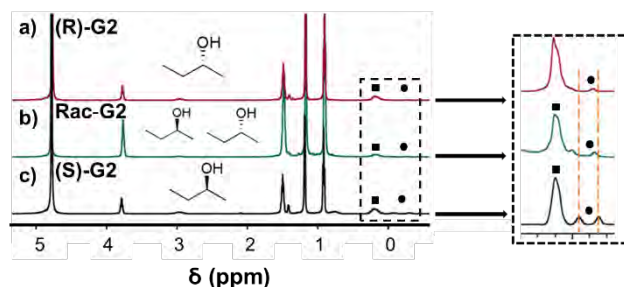
Figure 5. ^{1}H NMR spectra of two enantiomers of G2 • 1 and racemic-G2. **(a)** (R)-G2, **(b)** (S)/(R)-G2 and **(c)** (S)-G2 showing upfield signals of bound G2 (600 MHz, D₂O, 25 °C). ■ (Lactate in), ● (encapsulated G2).

This is confirmed by the distinct association constants of (R)-G2 and (S)-G2 with **L-1** at 25 °C. As shown in Table 1, the association constant of (S)-G2 to **L-1** (K_S) is three times of that of (R)-G2 (K_R). This enantioselectivity is greatly improved in comparison with G1 guests, indicating a better chiral recognition environment endowed by the confined cavity functionalized with chiral lactates. As the host-guest exchange is slow on NMR timescale, it was possible to easily distinguish between free and bound G2, subsequently determine the concentration of each species by integration of their NMR signals, and thus calculate the association constants. In either case, there was no observed increased uptake of the guest molecules in relation to increasing the temperature of the solutions.

Table 1. Recognition site, association constant and selectivity of L-G1, D-G1, (R)-G2 and (S)-G2 with **L-1**.

Recognition site	Association constant (M[-1])		Selectivity
Surface Pores	K_D (D-G1)	K_L (L-G1)	K_D/K_L
	1300±0.8	950±0.6	1.4
Interior Cavity	K_S (S-G2)	K_R (R-G2)	K_S/K_R
	473±0.4	158±0.3	3.0

In conclusion, we have reported the synthesis of chiral inorganic capsules **L-1** and **D-1**, functionalized by chiral lactate ligands, and their chiral recognitions towards L/D-carnitine and (R)/(S)-2-butanol in solution, for the first time. Based on two distinct recognition

sites in **L-1** and **D-1**, varied enantioselectivities are achieved. Distinct discrimination of the two enantiomers of 2-butanol ($K_S/K_R = 3$) is obtained when the recognition occurs within the cavity lined by lactates, while weaker differentiation is observed for L-carnitine and D-carnitine where the interactive surface pores are not proximal to the chiral ligands.

ASSOCIATED CONTENT

Supporting Information

The Supporting Information (experimental details, complete data tables, and plots) is available free of charge on the ACS Publications website.

AUTHOR INFORMATION

Corresponding Author

Leroy Cronin, Lee.Cronin@glasgow.ac.uk, School of Chemistry, University of Glasgow, Glasgow G12 8QQ, United Kingdom.

Author Contributions

LC conceived the idea and together with NW designed the project. NW devised the experimental approach, procedure and data interpretation. NW and ZS performed the chemistry and chemical analysis with respect to IR, UV-vis-NIR, elemental analysis, TGA, and NMR. WX performed CD study and X-ray analysis. RP helped performing experiments. DL completed structure elucidation. LC, NW, RP and YMA-H co-wrote the manuscript with input from all co-authors.

Notes

The authors declare no competing financial interests.

REFERENCES

(1) M. Rekharsky, Y. Inoue. Chiral Recognition Thermodynamics of β-Cyclodextrin: The Thermodynamic Origin of Enantioselectivity and the Enthalpy−Entropy Compensation Effect. *J. Am. Chem. Soc.* **2000**, *122*, 4418–4435.

(2) H. J. Kim, M. H. Lee, L. Mutihac, J. Vicens, J. S. Kim. Host–Guest Sensing by Calixarenes on the Surfaces. *Chem. Soc. Rev.* **2012**, *41*, 1173–1190.

(3) W.-H. Huang, P. Y. Zavalij, L. Isaacs. Chiral Recognition inside a Chiral Cucurbituril. *Angew. Chem. Int. Ed.* **2007**, *46*, 7425–7427.

(4) M. Sawada, Y. Takai, H. Yamada, S. Hirayama, T. Kaneda, T. Tanaka, K. Kamada, T. Mizooku, S. Takeuchi, Chiral Recognition in Host-Guest Complexation Determined by the Enantiomer-Labeled Guest Method Using Fast Atom Bombardment Mass Spectrometry. *J. Am. Chem. Soc.* **1995**, *117*, 7726–7736.

(5) Y. Nishioka, T. Yamaguchi, M. Kawano, M. Fujita. Asymmetric [2 + 2] Olefin Cross Photoaddition in a Self-Assembled Host with Remote Chiral Auxiliaries. *J. Am. Chem. Soc.* **2008**, *130*, 8160–8161.

(6) H. Zang, H. N. Miras, J. Yan, D. L. Long, L. Cronin. Assembly and Autochirogenesis of a Chiral Inorganic Polythioanion Möbius Strip via Symmetry Breaking. *J. Am. Chem. Soc.* **2012**, *134*, 11376–11379.

(7) X. Fang, T. M. Anderson, C. L. Hill. Enantiomerically Pure Polytungstates: Chirality Transfer through Zirconium Coordination Centers to Nanosized Inorganic Clusters *Angew. Chem. Int. Ed.* **2005**, *44*, 3540–3544.

(8) W. Xuan, R. Pow, N. Watfa, Q. Zheng, A. J. Surman, D. long, L. Cronin. Stereoselective Assembly of Gigantic Chiral Molybdenum Blue Wheels Using Lanthanide Ions and Amino Acids *J. Am. Chem. Soc.* **2019**, *141*, 1242-1250.

(9) A. Müller, E. Krickemeyer, H. Bögge, M. Schmidtmann, F. Peters. Organizational Forms of Matter: An Inorganic Super Fullerene and Keplerate Based on Molybdenum Oxide. *Angew. Chem. Int. Ed.* **1998**, *37*, 3359–3363.

(10) (a) A. Grego, A. Müller, I. A. Weinstock. Stepwise-Resolved Thermodynamics of Hydrophobic Self-Assembly. *Angew. Chem. Int. Ed.* **2013**, *52*, 8358–8362 (b) C. Schäffer, H. Bögge, A. Merca, I. A. Weinstock, D. Rehder, E. T. K. Haupt, A. Müller. A Spherical 24 Butyrate Aggregate with a Hydrophobic Cavity in a Capsule with Flexible Pores: Confinement Effects and Uptake–Release Equilibria at Elevated Temperatures. *Angew. Chem. Int. Ed.* **2009**, *48*, 8051–8056. (c) T.-L. Lai, M. Awada, S. Floquet, C. Roch-Marchal, N. Watfa, J. Marrot, M. Haouas, F. Taulelle, E. Cadot. Tunable Keplerate Type-Cluster "Mo_{132}" Cavity with Dicarboxylate Anions. *Chem. Eur. J.* **2015**, *21*, 13311–13320.

(11) (a) N. Watfa, *et al*. Two Compartmentalized Inner Receptors for the Tetramethylammonium Guest within a Keplerate-Type Capsule. *Inorg. Chem.* **2016**, *55*, 9368-9376. (b) N. Watfa, D. Melgar, M. Haouas, F. Taulelle, A. Hijazi, D. Naoufal, J. B. Avalos, S. Floquet, C. Bo, E. Cadot. Hydrophobic Effect as a Driving Force for Host–Guest Chemistry of a Multi-Receptor Keplerate-Type Capsule. *J. Am. Chem. Soc.* **2015**, *137*, 5845–5851.

(12) A. Müller, E. Krickemeyer, H. Bögge, M. Schmidtmann, S. Roy, A. Berkle. Changeable Pore Sizes Allowing Effective and Specific Recognition by a Molybdenum-Oxide Based "Nanosponge": En Route to Sphere-Surface and Nanoporous-Cluster Chemistry. *Angew. Chem. Int. Ed.* **2002**, *41*, 3604–3609.

(13) A. Müller, L. Toma, H. Bögge, C. Schäffer, A. Stammler. Porous Capsules Allow Pore Opening and Closing That Results in Cation Uptake. *Angew. Chem. Int. Ed.* **2005**, *44*, 7757–7761.

(14) (a) S. Kopilevich, H. Gottlieb, K. Keinan-Adamsky, A. Müller, I. A. Weinstock. The Uptake and Assembly of Alkanes within a Porous Nanocapsule in Water: New Information about Hydrophobic Confinement. *Angew. Chem. Int. Ed.* **2016**, *55*, 4476–4481. (b) B. B. Sarma, L. Avram, R. Neumann. Encapsulation of Arenes within a Porous Molybdenum Oxide {Mo_{132}} Nanocapsule. *Chem. Eur. J.* **2016**, *22*, 15231–15236.

(15) A. Müller, E. Krickemeyer, H. Bögge, M. Schmidtmann, B. Botar, M. O. Talismanova. Drawing Small Cations into Highly Charged Porous Nanocontainers Reveals "Water" Assembly and Related Interaction Problems. *Angew. Chem. Int. Ed.* **2003**, *42*, 2085–2090.

Enantioselective Recognition of Chiral Guests by the Water-Soluble Chiral [Mo$_{132}$O$_{372}$(H$_2$O)$_{72}$(x-Lactate)$_{30}$]$^{42-}$ Nanocapsules.

Nancy Watfa[‡], Weimin Xuan, Zoë Sinclair, Robert Pow, Yousef M. Abul-Haija, De-Liang Long and Leroy Cronin*

School of Chemistry, University of Glasgow, Glasgow G12 8QQ, UK

* Corresponding author: Leroy Cronin lee.cronin@glasgow.ac.uk;

Contents

1. Materials and Instrumentation

Unless noted otherwise, reagent-grade chemicals were obtained from commercial suppliers (Aldrich Chemical Company Ltd. and Alfa Aesar) and used without further purification. $(NH_4)_{42}[Mo_{132}O_{372}(H_2O)_{72}(CH_3COO)_{30}].150H_2O$ (noted {Mo_{132}}-acetate) and $(NH_4)_{72}[Mo_{132}O_{372}(H_2O)_{72}(SO_4)_{30}].200H_2O$ (noted {Mo_{132}}-sulfate) were prepared according to a previously reported method and characterized by ^{1}H NMR and IR. [1,2]

Single Crystal X-ray Crystallography: A suitable single crystal was selected and mounted onto a rubber loop using Fomblin oil. X-ray diffraction intensity data was collected on a Bruker Apex II Quasar CCD diffractometer (λ (MoK_α) = 0.71073 Å) equipped with a microfocus X-ray source (50 kV, 1.0 mA). Data collection and reduction were performed using the Apex2 software package and structure solution and refinement were carried out using SHELXS-2016[3] and SHELXL-2018[4] using the WinGX suite. Corrections for incident and diffracted beam absorption effects were applied using empirical absorption correction. All the Mo atoms (including those disordered) and most of the O atoms were refined anisotropically. Solvent water molecule sites with partial occupancy were found and included in the structure refinement. Crystallographic formulae typically contain much more water molecules in the crystal lattice than the formulae determined from chemical analyses as the samples are dried for the latter analyses. It is important to note that with these large structures we are moving outside the realm of small molecule crystallography and are dealing with refinements and problems that lie between small molecule and protein crystallography. As a result, we cannot expect refinements and statistics to follow the path of crystals with much smaller unit cells. However, the final refinement statistics are relatively good, and in all cases the structural analysis allows us to determine to a significant extent the structures of the compounds. The X-ray crystallographic data reported in this article have been deposited at the Crystallographic Data Centres. For compound **L-1**, the data can be obtained free of charge from the Cambridge Crystallographic Data Centre via www.ccdc.cam.ac.uk/data_request/cif under deposition number CCDC-1898694.

Fourier-Transform Infrared (FT-IR) Spectroscopy: The samples were prepared as a KBr pellet and the FT-IR spectrum was collected in transmission mode in the range of 400-2500 cm^{-1} using a JASCO FT-IR 4100 spectrometer. Wavenumbers are given in cm^{-1}. Intensities are denoted as w = weak, m = medium, s = strong, br = broad, sh = sharp.

Elemental Analyses: Element analyses for Mo and S were performed on a Leeman inductively-coupled plasma (ICP) spectrometer while C, N and H content were determined by

the microanalysis services within the School of Chemistry, University of Glasgow, using an EA 1110 CHNS, CE-440 Elemental Analyzer.

Thermogravimetric Analysis (TGA): Thermogravimetric analysis was performed on a TA Instruments Q 500 Thermogravimetric Analyzer under nitrogen flow at a typical heating rate of 10 °C min^{-1}.

NMR Procedure: The analyses were performed on a Bruker Ascend Aeon 600 MHz NMR spectrometer equipped with a room temperature BBFO probe head. Standard ^{1}H NMR spectra measurements were performed at 300 K and NMR chemical shifts were referenced to TMS as an external standard (d = 0 ppm). Diffusion measurements were performed using LED (longitudinal eddy current delay) diffusion sequence: the duration of the pulse field gradients (δ) applied to encode and decode the diffusion was set to 1.2 ms. The diffusion time for the experiment (Δ) was optimized between Δ = 75−100 ms. The raw data were processed using the Dynamics Center program (Bruker) and data were fit to Equation 1 in which I and I_0 are the echo intensity in the presence and absence of the gradient pulse, respectively, γ is the gyromagnetic ratio, G is the pulse gradient strength, δ is the length of pulse gradient, τ is the gradient stabilization delay, Δ is the time interval between the leading edges of the pulse-gradient used, and D is the diffusion coefficient.

$$\ln I/ I_0 = - \gamma^2\, \delta^2\, G^2[\Delta-(4\delta/3)]D = -bD \qquad (Equation\ 1)$$

2. Synthesis of L-1 and D-1

Compounds **L-1** and **D-1** were prepared following the same procedure. An excess of L- or D-lactate (0.35 g, 3.88 mmol) was added directly into 15 ml of {Mo$_{132}$}-sulfate (0.5 g, 0.0178 mmol) -previously prepared according to reference [2] - with the pH controlled to 3.8 using hydrochloric acid (1M). The resulting solution was stirred for one hour. Then, ammonium chloride (0.5 g, 9.35 mmol) was added and the solution was stirred again for another 10 min before being transferred to an open beaker for crystallization. After one-week, dark brown crystals appeared and were filtered and washed with ethanol and diethyl ether.

For L-1: $(NH_4)_{49}[Mo_{132}O_{372}(H_2O)_{72}(C_3H_5O_3)_{30}](C_3H_5O_3)_5(SO_4)(H_2O)_{220}$

Yield (0.30 g, 60%).

Elemental analysis, calc.: C, 4.51%; H, 3.44 %; N, 2.45 %; Mo, 45.3 %; S, 0.11 %; found: C, 4.50 %; H, 3.20 %; N, 2.50 %; Mo, 45.5 %; S, 0.13 %.

IR (KBr pellet, 2500–400 cm^{-1}): 1616 (w), 1556 (m), 1423 (m), 1130 (w), 972 (s), 935 (m), 854 (w), 790 (s), 704 (s), 630.72 (w), 561.28 (m), 472 (w).

For D-1: $(NH_4)_{46}[Mo_{132}O_{372}(H_2O)_{72}(C_3H_5O_3)_{30}](SO_4)_2(H_2O)_{250}.$

Yield (0.30 g, 60%).

Elemental analysis, calc.: C, 3.84 %; H, 3.51%; N, 2.29 %; Mo, 45.1 %; S, 0.23 %; found: C, 3.86 %; H, 3.15 %; N, 2.29 %; Mo, 45.5 %; S, 0.24 %.

IR (KBr pellet, 2500–400 cm^{-1}): 1620 (w), 1550 (m), 1429 (m), 11347 (w), 972 (s), 935 (w, sh), 854 (w), 785 (m), 700 (m), 630.72 (w), 557.42 (s), 468 (w).

Ligand-Exchange of D/L-Lactate with {Mo$_{132}$}-acetate

To probe the ligand exchange of either L-Lactate or D-Lactate with ligands present on {Mo$_{132}$} by ^{1}H NMR measurements, we have used the {Mo$_{132}$}-acetate structure as the precursor molecule – prepared according to reference [1] as observable proton signal related to the acetate ligand can be obtained. The number of equivalents of D/L-lactate is given relative to the concentration of the {Mo$_{132}$}-acetate structure.
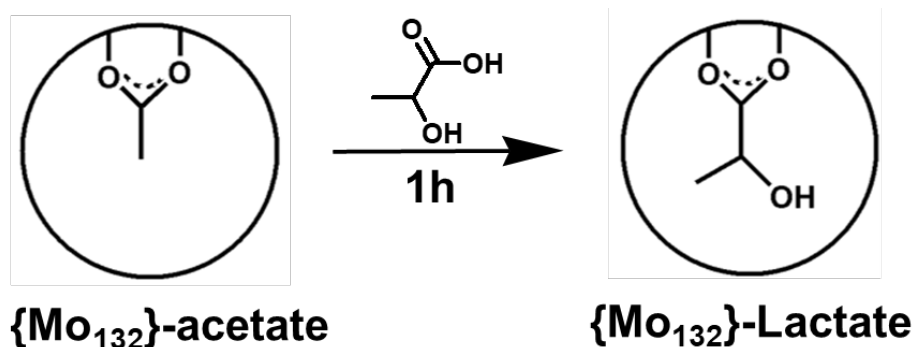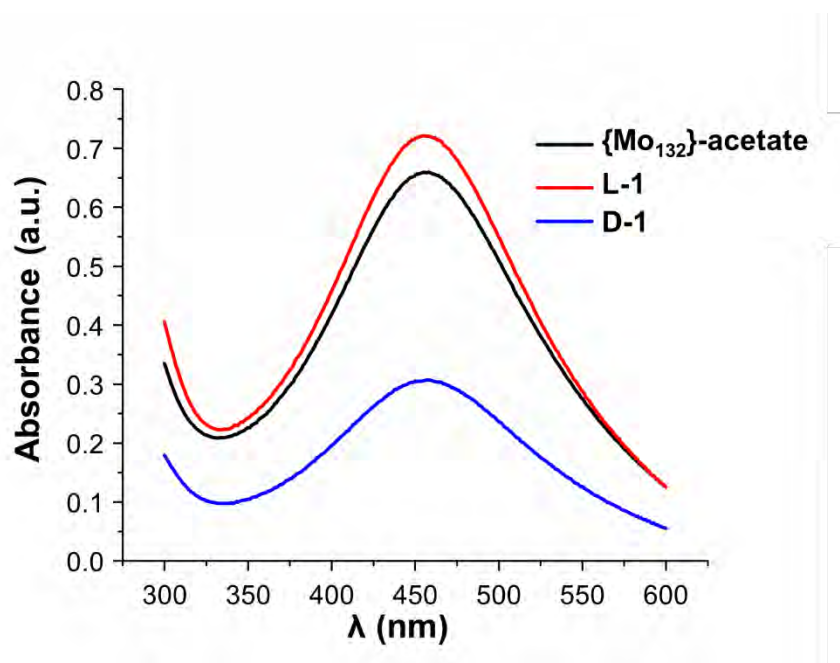

Scheme 1. Schematic representation of the replacement of acetate ligands by lactate ligands.
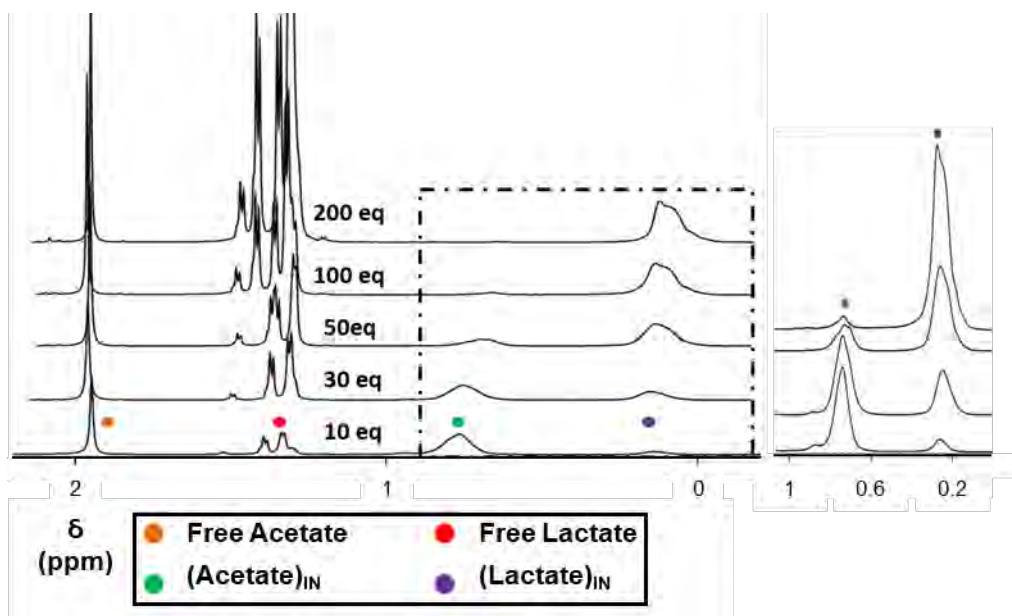
Figure S1. ^{1}H NMR {Mo$_{132}$}-acetate in the presence of different ratios of L-lactate.

3. Spectral Characterization of Chiral Keplerate

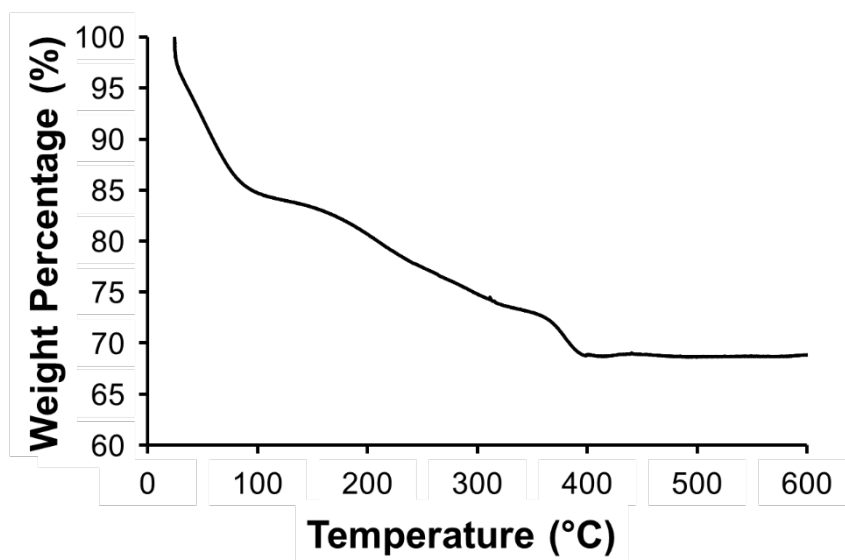**Figure S2.** UV-vis-NIR spectra of **L-1** and **D-1**, in comparison to {Mo$_{132}$}-acetate.

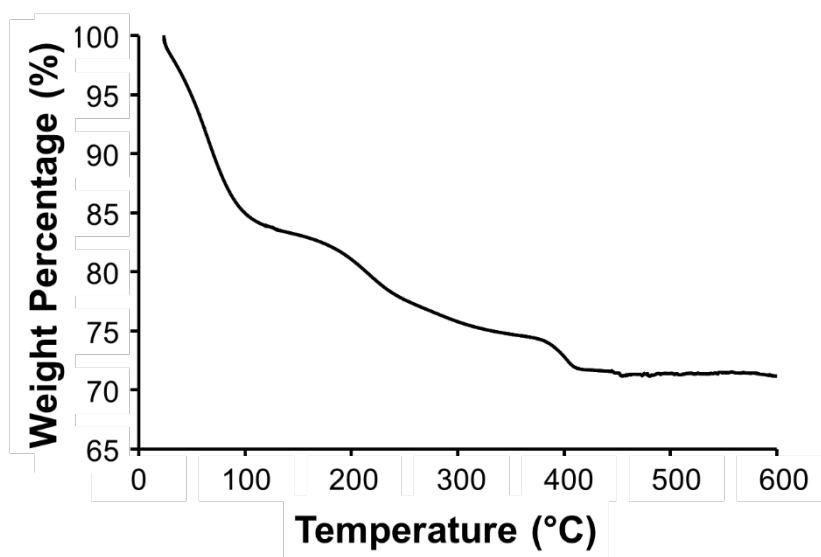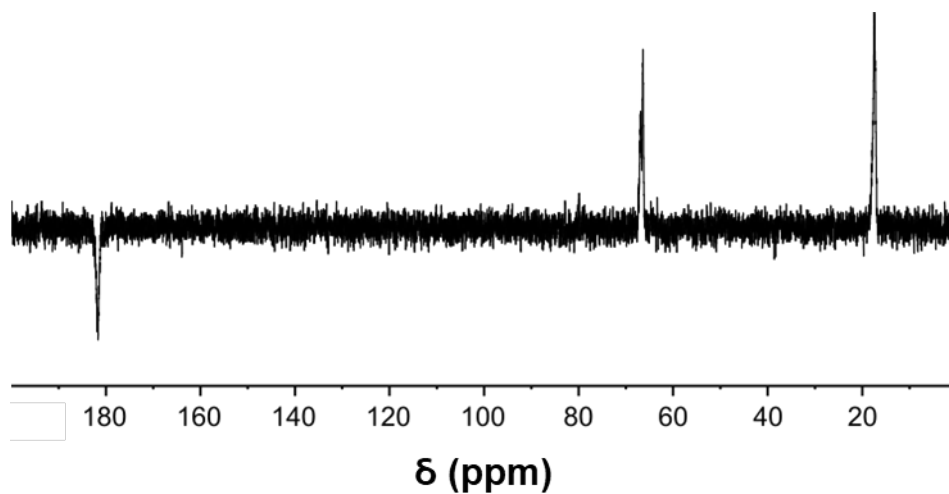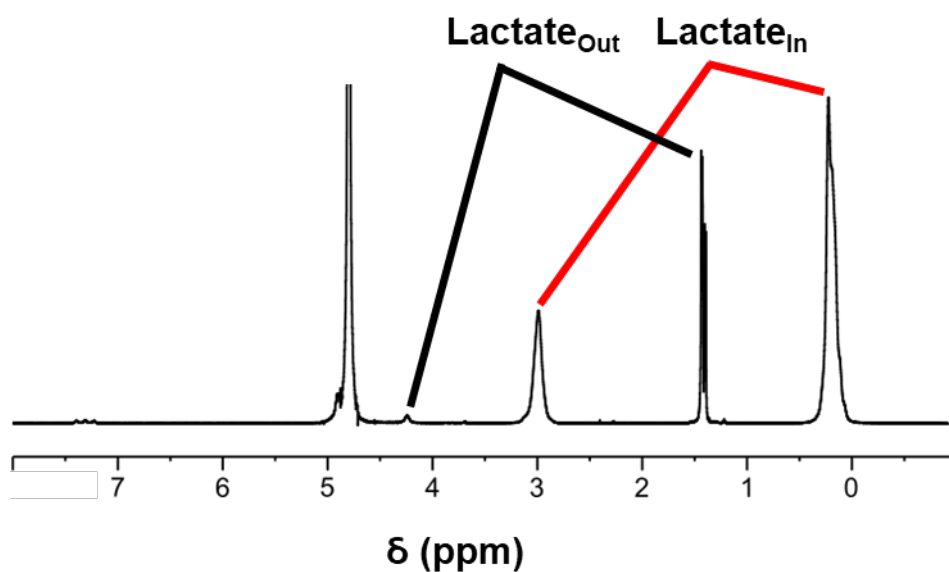**Figure S3.** TGA curve for compound **L-1**.

Figure S4. TGA curve for compound **D-1**.

4. NMR Characterization of L-1 and D-1.

Figure S5. ^{13}C-DEPTQ NMR of **L-1** in D_2O. Phase down signals are attributed to non-protonated carbons (C) and methylene carbons (CH_2), while the relative antiphase signals (pointing up) are attributed to methine (CH) and methyl carbons (CH_3).

Figure S6. ^1H NMR spectrum of **L-1** showing both encapsulated and free L-lactate ligands (600 MHz, D_2O, 25 °C).
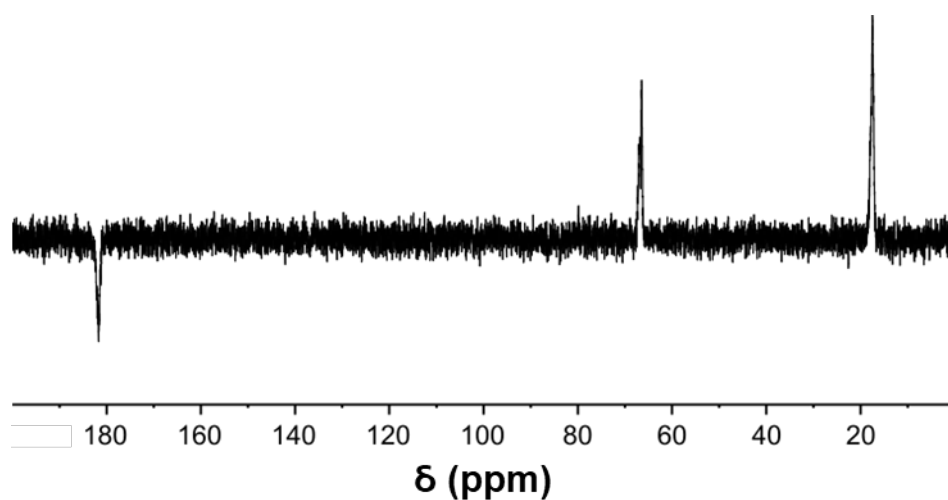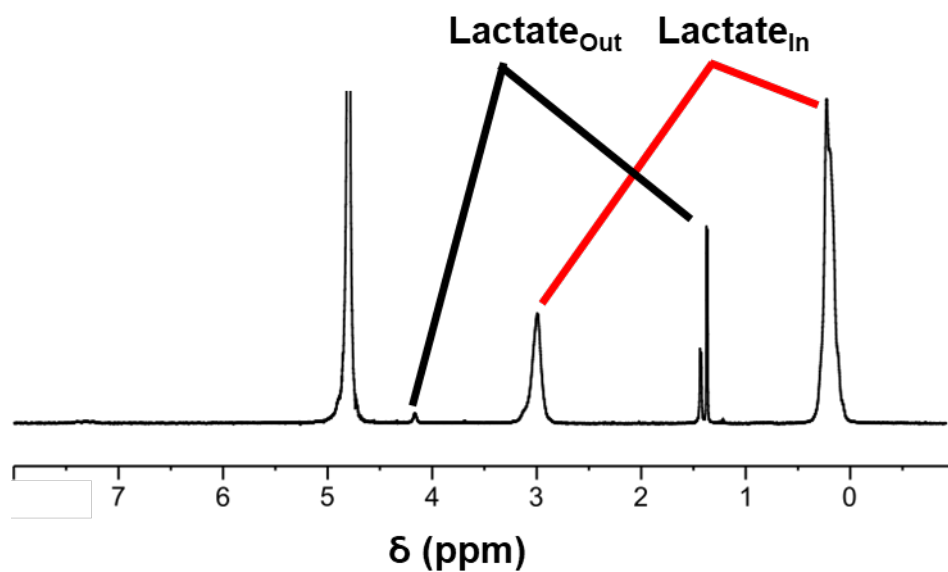
Figure S7. ^{13}C-DEPTQ NMR of **D-1** in D_2O. Phase down signals are attributed to non-protonated carbons (C) and methylene carbons (CH_2), while the relative antiphase signals (pointing up) are attributed to methine (CH) and methyl carbons (CH_3).
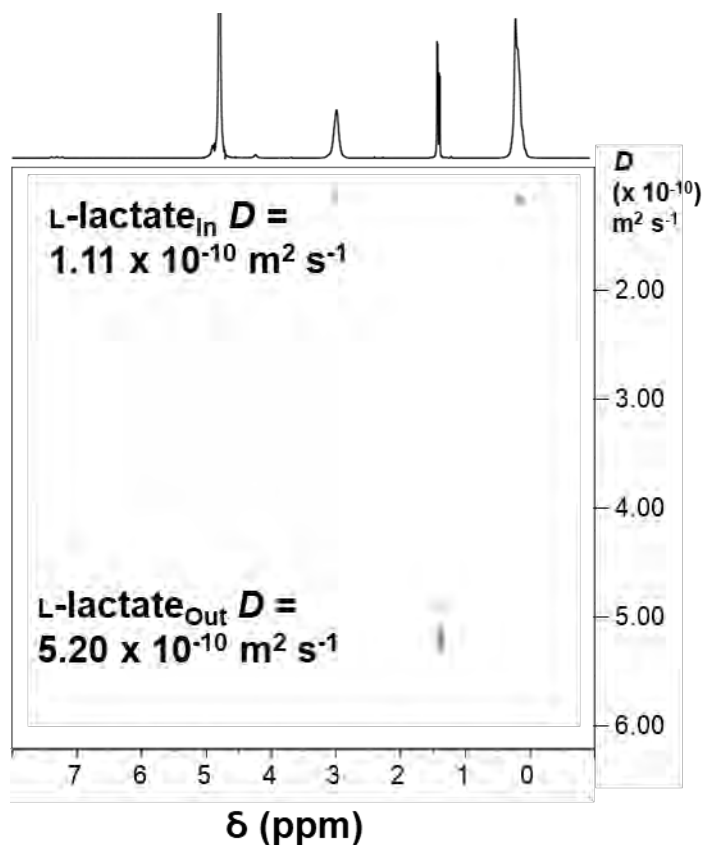

Figure S8. ^{1}H NMR spectrum of **D-1** showing both encapsulated and free D-lactate ligands (600 MHz, D_2O, 25 °C).

**Figure S9.** ^{1}H DOSY NMR of **L-1** in D_2O.

5. Chiral Recognition Studies by ^{1}H NMR Experiments

5.1 Recognition at {Mo$_{132}$} Pores

Sample preparation for NMR measurement: two separate stock solutions were prepared in D_2O: one with 200 mg of either **L-1** or **D-1** (10 mM, 0.75 ml), and one containing 7.0 mg of L- or D-carnitine hydrochloride (50 mM, 0.75 ml). Combination of these stock solutions in a 1:1 ratio results in a solution with {Mo$_{132}$}:L-/D-carnitine in a 1:5 ratio. This mixed solution was stirred for 5 min. From this mixed solution, a series of diluted solutions of decreasing overall {Mo$_{132}$} concentration (from 5 mM to 0.1875 mM) were prepared by taking an appropriate aliquot of the mixed solution and adding D_2O to a total final volume of 1 ml.
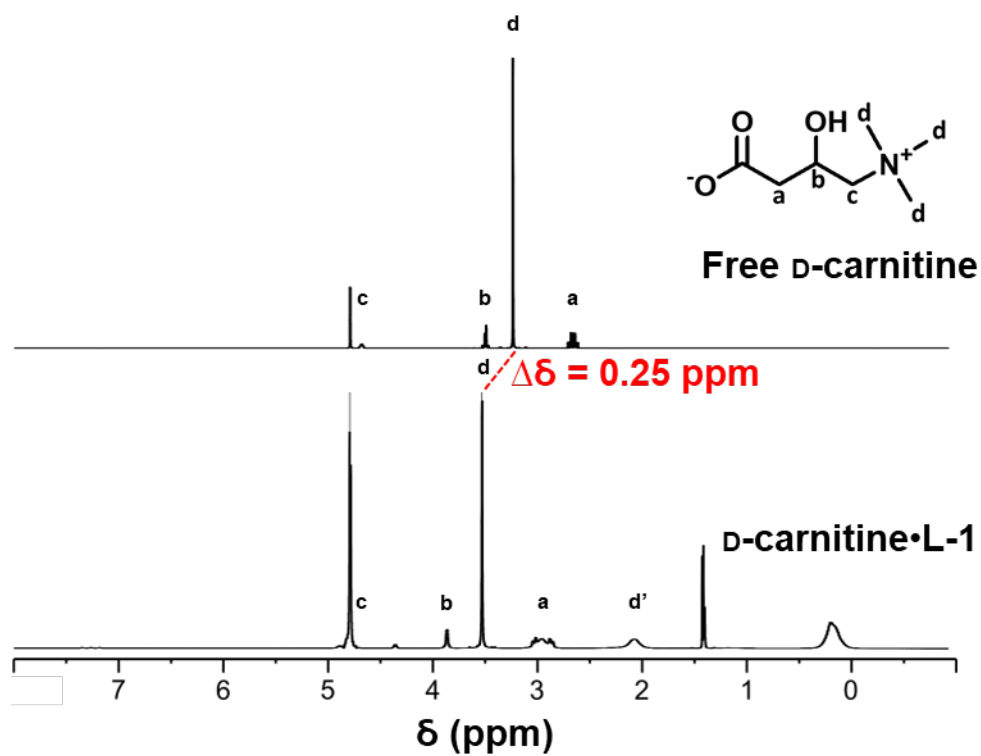
Figure S10. ^{1}H NMR spectrum of free D-carnitine and D-carnitine • L-1. Downfield shifts ($\Delta\delta = 0.25$ ppm) of all free carnitine peaks is observed. In addition, a broadened peak appearing at approximately 2.1 ppm, associated with the interaction of the CH_3 methyl protons of the amide group with the Keplerate pore, is present (600 MHz, D_2O, 25 °C).
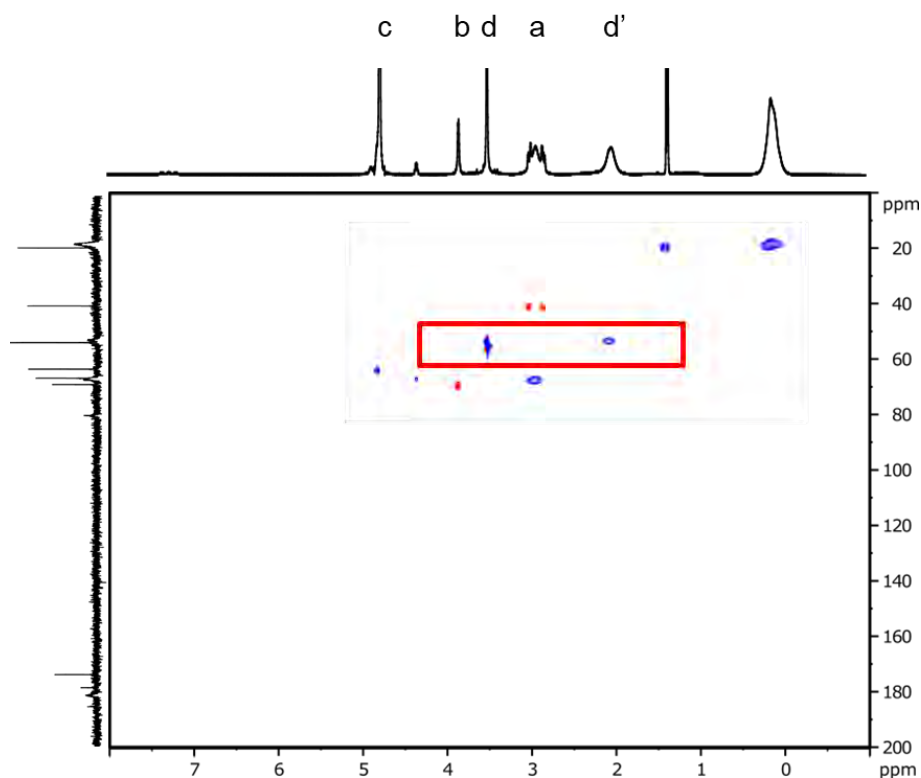
Figure S11. Two-dimensional phase-sensitive Heteronuclear Single-Quantum Correlation (HSQC) spectrum of D-carnitine • L-1 (600 MHz, 300 K). The highlighted box shows that the broadened peak at 2.1 ppm originates from the broadened carbon signal of the methyl groups coordinated to the amide of the L-carnitine, whilst the signal retains its multiplicity. The positive signals (red) are related to CH_2 protons, while the negative signals (blue) are related to CH and CH_3 proton signals.
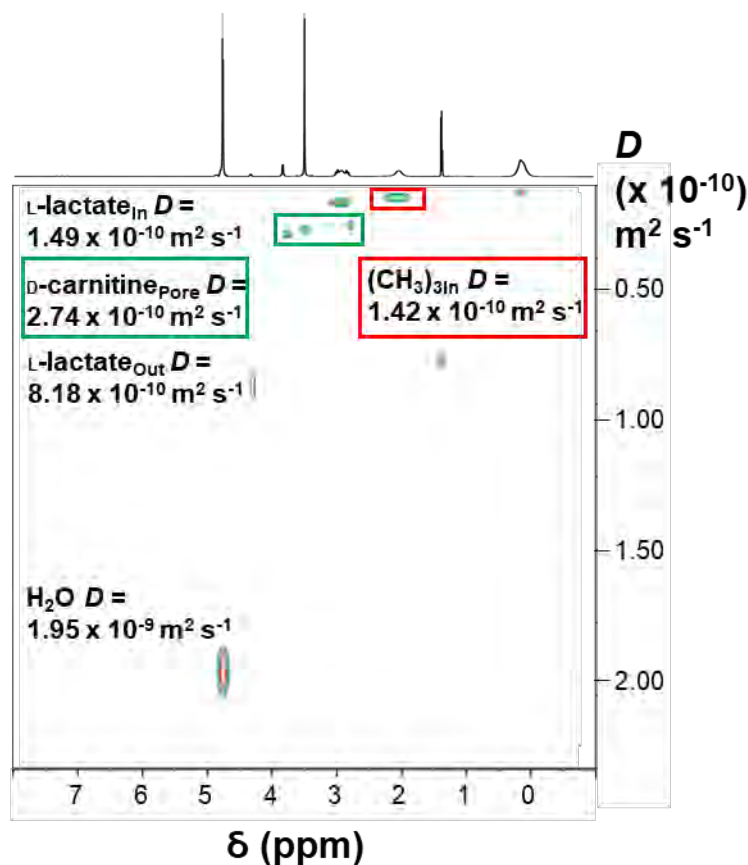
Figure S12. Two-dimensional diffusion spectrum of D-carnitine ● **L-1** in D_2O (600 MHz, 300 K).

Pore Binding Model - Competition between Cations and Guests

The presence of shifted carnitine peaks, with no separate broadened resonances, is indicative of a fast exchange, on the NMR timescale, of the interaction of carnitine with the pores of $\{Mo_{132}\}$. The observed time-averaged diffusion coefficient of the carnitine ligands, D_{obs}, is given by the weighted-average of the guest in both the free and complexed states according to equation 2:

$$D_{obs} = \chi_{bound}D_{bound} + (1 - \chi_{bound})D_{free} \; (equation \; 2)$$

Where, χ_{bound} is the mole fraction of the guest in the bound state, and hence $(1 - \chi_{bound})$ represents the mole fraction of the free guest. D is the diffusion coefficient of the guest in the free or bound state. The diffusion coefficient for the fully bound guest is effectively the same as the diffusion coefficient of the host, due to the large difference in the size of the two species and the subsequently negligible effect that the interaction has on the diffusion coefficient of

12

the host. Explicitly therefore, D_{bound} is equal to the diffusion coefficient of the $\{Mo_{132}\}$, which can be derived from the diffusion coefficient of the encapsulated lactate ligands (115 m^{2}s^{-1}), which are in a slow-exchange process. Equation 2 can be rearranged to derive a value of χ_{bound} by equation 3.

$$\chi_{bound} = \frac{D_{free} - D_{obs}}{D_{free} - D_{bound}} \ (equation\ 3)$$

Where D_{free} is the diffusion coefficient of free carnitine (800 m^2 s^{-1}), D_{obs} is the observed diffusion coefficient of L-carnitine or D-carnitine, and D_{bound} is the diffusion coefficient of **L-1** and **D-1** (115 m^{2}s^{-1}).

The binding sites, the 20 $\{Mo_{132}\}$ pores, are assumed to be independent of one another (primarily due to the significant distance between any two proximal sites) and their subsequent individual binding affinities are not influenced by the presence of absence of guests at other binding sites. Competition between two separate species, ammonium cations present as counterions (49 mol^{-1} for **L-1**, and 46 mol^{-1} for **D-2**) and our added carnitine guests, binding at the pores is expected.

This competition for binding sites allows for the establishment of equilibrium conditions between the two competing species and the binding sites. For the $\{Mo_{132}\}$ host with 20 surface pores, equilibria are established between these free sites, [H], with free carnitine [G1], and free ammonium guests [G2]. The concentration of bound guests to the pore sites is denoted as [HG1] and [HG2], for the binding of carnitine or ammonium cations to $\{Mo_{132}\}$, respectively.

$$[H] + [G1] \rightleftharpoons [\text{HG1}] \ (equation\ 4)$$

$$[H] + [G2] \rightleftharpoons [\text{HG2}] \ (equation\ 5)$$

Separate association constants (K1 and K2) can then be derived for equations (4) and (5), with respect to the concentrations of the interacting species:

$$K1 = \frac{[HG1]}{[H][G1]} \ (equation\ 6)$$

$$K2 = \frac{[HG2]}{[H][G2]} \ (equation\ 7)$$

The number of equivalents of guests, carnitine (G1) or ammonium cations (G2), relative to the concentration of $\{Mo_{132}\}$ can be described by the following equations, 7, 8, and 9. As previously stated, the number of $\{Mo_9O_9\}$ pores in the $\{Mo_{132}\}$ structure is known to be 20. Using the concentration of $\{Mo_{132}\}$ (denoted by $C°$), the concentration of pores is given by $20C°$. This is equitable to the sum of all possible complexes of $\{Mo_{132}\}$ ([H], [HG1], and [HG2]) in the given system (equation 8). The number of equivalents, with respect to $C°$, of carnitine (G1) added to a solution of $\{Mo_{132}\}$ was 5. The number of ammonium cations in **L-1** is derived from earlier chemical and structural analyses and is found to be 49 (therefore the concentration is given by $49C°$). These two statements result in equations 9 and 10 being constructed, respectively, based on the same reasoning as equation 8.

$$20C° = [H] + [HG1] + [HG2] (equation\ 8)$$

$$5C° = [G1] + [HG1]\ (equation\ 9)$$

$$49C° = [G2] + [HG2]\ (equation\ 10)$$

In such conditions, and whatever the concentration $C°$, [HG1] is negligible compared to the sum of [H] and [HG2]. This means that the concentration, [HG1], can be neglected with respect to this sum and equation 8 is then simplified into equation 11.

$$20C° = [H] + [HG2]\ (equation\ 11)$$

Following several equation rearrangements, substitutions and the application of the conversation of mass within our given system, equations 7, 10 and 11 may be used to form a quadratic equation with $x = [HG2]$, equation 13. This is followed by the deduction of the positive root of [HG2] by use of the quadratic formula in equation 14. The method for this is shown below, firstly restating the essential equations previously constructed and both mathematical formulas required to solve for [HG2].

$$K2 = \frac{[HG2]}{[H][G2]}\ (equation\ 7)$$

$$49C° = [G2] + [HG2]\ (equation\ 10)$$

$$20C° = [H] + [HG2]\ (equation\ 11)$$

$$ax^2 + bx + c = 0\ (the\ general\ formula\ of\ the\ quadratic\ equation, equation\ 12)$$

$$a[HG2]^2 + b[HG2] + c = 0 \ (equation \ 13)$$

$$x = \frac{-b \pm \sqrt{(b^2 - 4ac)}}{2a} \ (the \ quadratic \ formula, equation \ 14)$$

The first step is to rearrange equations 10 and 11, our mass balance relationships, to solve for [G2] and [H] respectively. Explicitly, equation 10 can be rearranged to give [G2] and [HG2], resulting in equations 15 and 16, while equation 11 can be rearranged to equation 17, to give [H].

$$[G2] = 49C° - [HG2] \ (equation \ 15)$$

$$49C° = [G2] + [HG2] \ (equation \ 10)$$

$$[HG2] = 49C° - [G2] \ (equation \ 16)$$

$$20C° = [H] + [HG2] \ (equation \ 11) \longrightarrow [H] = 20C° - [HG2] \ (equation \ 17)$$

Then taking equation 7, the association constant relationship, and substituting in equations 15, 16 and 17 to remove any [G2] terms, we obtain equation 18.

$$K2 = \frac{[HG2]}{[H][G2]} \ (equation \ 7)$$

$$K2 = \frac{[HG2]}{(20C° - [HG2])(49C° - [HG2])} \ (equation \ 18)$$

Multiplying out equation 18 to remove the fraction and the two brackets on the denominator, results in our quadratic equation in [HG2], equation 19.

$$K2 = \frac{[HG2]}{(20C° - [HG2])(49C° - [HG2])} \ (equation \ 18)$$

$$\frac{[HG2]}{(980C° - 20C°[HG2] - 49C°[HG2] + [HG2]^2)} = K2$$

$$[HG2] = K2(980C° - 69C°[HG2] + [HG2]^2)$$

$$980C°^2K2 - 69C°K2[HG2] + K2[HG2]^2 - [HG2] = 0$$

$$K2[HG2]^2 - 69C°K2[HG2] - [HG2] + 980C°^2K2 = 0$$

$$K2[HG2]^2 - (69C°K2 + 1)[HG2] + 980C°^2K2 = 0 \ (equation\ 19)$$

Using equation 19, in the form of $ax^2 + bx + c = 0$, we can solve our quadratic equation for values of a, b and c remembering that $x = [HG2]$:

$$a = K2, b = -(69C°K2 + 1), c = 980C°^2K2 \ (equation\ 20)$$

Now, with known values of C° and [G2], and taking a set value of K2 (= 200 M^{-1}), a value of [HG2] can be established by solving for only the positive root of the quadratic formula given in equation 14, resulting in equation 21.

$$x \ \frac{-b \ \pm \ \sqrt{(b^2 - 4ac)}}{2a} \ (equation\ 14)$$

$$[HG2] = \frac{(69C°K2 + 1) + \sqrt{(-(69C°K2 + 1))^2 - 4K2(980C°^2K2)}}{2K2} \ (equation\ 21)$$

A known value of [HG2] then allows for determination of [G2] from equation 15.

$$[G2] = 49C° - [HG2] \ (equation\ 15)$$

Following a similar procedure, we can achieve a similar expression for the association constant (K1) of carnitine with {Mo$_{132}$}. Taking equation 9 and rearranging for [HG1], to give equation 22, and taking equation 7 and rearranging for [HG2], to give equation 23, then substituting them both into equation 8, we can obtain equation 24 which can be rearranged for [H]:

$$5C° \ = \ [G1] + [HG1] \ (equation\ 9) \quad \longrightarrow \quad [HG1] = 5C° - [G1] \ (equation\ 22)$$

$$K2 = \frac{[HG2]}{[H][G2]} \ (equation\ 7)$$

$$[HG2] = K2([H][G2]) \ \ (equation\ 23)$$

$$20C° \ = \ [H] + [HG1] + [HG2] \ \ (equation\ 8)$$

$$20C° \ = \ [H] + (5C° - [G1]) \ + K2([H][G2])$$

$$20C° \ = \ [H] + 5C° - [G1] \ + K2[H][G2] \ (equation\ 24)$$

By taking equation 24 and collecting like terms, [H], then multiplying out brackets we can obtain an expression for [H] – our concentration of $\{Mo_{132}\}$ – equation 25.

$$[H] = 20C° - 5C° + [G1] - K2[H][G2] \; (rearranged\; version\; of\; equation\; 24)$$

$$[H] + K2[H][G2] = (20 - 5)C° + [G1]$$

$$[H](1 + K2[G2]) = (20 - 5)C° + [G1]$$

$$[H] = \frac{[G1] + (20 - 5)C°}{(1 + K2[G2])} \; (equation\; 25)$$

Now with an expression for [H] we can find a relationship for association constant, K1 by substituting in equation 22 and 25 to equation 6:

$$K1 = \frac{[HG1]}{[H][G1]} \; (equation\; 6)$$

$$[HG1] = 5C° - [G1] \; (equation\; 22)$$

$$[H] = \frac{[G1] + (20 - 5)C°}{(1 + K2[G2])} \; (equation\; 25)$$

$$K1 = \frac{5C° - [G1]}{\dfrac{[G1] + (20 - 5)C°}{(1 + K2[G2])}[G1]}$$

Multiplying out the denominator fraction leaves us with equation 26:

$$K1 = \frac{5C° - [G1]}{\dfrac{[G1]^2 + (20 - 5)C°[G1]}{(1 + K2[G2])}}$$

$$K1 = \frac{(5C° - [G1])(1 + K2[G2])}{[G1]^2 + (20 - 5)C°[G1]} \; (equation\; 26)$$

Removing the brackets from the numerator gives equation 27:

$$K1 = \frac{5C° + 5C°K2[G2] - [G1] - K2[G2][G1]}{[G1]^2 + (20 - 5)C°[G1]} \quad (equation\ 27)$$

Rearranging equation 27 to resemble the form of a quadratic equation, where $x = [G1]$, provides us with equation 28:

$$K1 = \frac{5C° + 5C°K2[G2] - [G1] - K2[G2][G1]}{[G1]^2 + (20 - 5)C°[G1]} \quad (equation\ 27)$$

$$5C° + 5C°K2[G2] - [G1] - [G2]K2[G1] = K1([G1]^2 + (20 - 5)C°[G1])$$

Rearranging to give the form $ax^2 + bx + c = 0$, where $x = [G1]$:

$$5C° + 5C°K2[G2] - [G1] - [G2]K2[G1] - K1[G1]^2 - (20 - 5)C°K1[G1] = 0$$

$$-K1[G1]^2 - [G1] - [G2]K2[G1] - (20 - 5)C°K1[G1] + 5C° + 5C°K2[G2] = 0$$

Now collecting like terms and multiplying by -1 we achieve equation 29:

$$-K1[G1]^2 - (1 + [G2]K2 + (20 - 5)C°K1)[G1] + 5C°(1 + K2[G2]) = 0$$

$$K1[G1]^2 + (1 + [G2]K2 + (20 - 5)C°K1)[G1] - 5C°(1 + K2[G2]) = 0 \ (equation\ 29)$$

Extracting a, b and c:

$$a' = K1, b' = (1 + [G2]K2 + (20 - 5)C°K1), c' = -5C°(1 + K2[G2]) \ (equation\ 30)$$

A value of [G1] can then be established by solving for only the positive root of the quadratic formula given in equation 14, resulting in equation 31.

$$x = \frac{-b \pm \sqrt{(b^2 - 4ac)}}{2a} \quad (equation\ 14)$$

$$[G1] =$$

$$\frac{-\left((1+[G2]K2+(20-5)C°K1)\right) + \sqrt{\left((1+[G2]K2+(20-5)C°K1)^2 - 4K1(-5C°(1+K2[G2]))\right)}}{2K1} \ (equation\ 31)$$

Now, with known values of C° and K2, a value of [HG2] and [G2] established from solving equation 21 previously, we can vary K1 to then produce values for [G1], and subsequently values for [HG1] by applying equation 22. Practically, this involves creating a table with a series of incrementally increasing $C°_{calc}$ values, then completing the known values previously mentioned, and finally varying K1 to derive values for [G1] and [HG1]. As discussed earlier, the observed diffusion coefficient for our guest (G1) is a weighted average of the guest in the free and bound states, as demonstrated by equation 2.

$$D_{obs} = \chi_{bound}D_{bound} + (1 - \chi_{bound})D_{free} \ (equation \ 2)$$

X_{bound}, the mole fraction of guests bound can more directly be stated as:

$$\frac{[HG1]}{[G1]} = \chi_{bound} \ (equation \ 32)$$

With known values of D_{bound}, D_{free}, D_{obs}, and the variation of K1 to derive values for [HG1] and [G1], a graph of $C°_{calc}$ versus D_{calc} can be generated (Fig. S13). Variation of the K1 value to produce a graph which retains the best fit of the calculated values of D_{calc} with D_{obs} (from tables S1-4) is carried out, with the most representative comparison used to confirm the final K1 value.

Table S1. Observed self-diffusion coefficient for L-carnitine in different **L-1** concentration

C° (mM)	D_{obs} (10^{-12} m^2. s^{-1})	χ_{bound}
3	300	0.73
2	313	0.70
1.3	343	0.66
0.6	360	0.64
0.15	546	0.37
0	800	0

Table S2. Observed self-diffusion coefficient for L-carnitine in different **D-1** concentration

C° (mM)	D_{obs} (10^{-12} m^2. s^{-1})	χ_{bound}
2	320	0.7
0.86	330	0.68
0.57	328	0.69
0.1875	416	0.64
0	800	0

Table S3. Observed self-diffusion coefficient for D-carnitine in different **L-1** concentration

C° (mM)	D_{obs} (10^{-12} m^2. s^{-1})	χ_{bound}
5	268	0.77
3	289	0.75
1.5	294	0.73
0.75	316	0.71
0.375	339	0.64
0.185	417	0.56
0	800	0

Table S4. Observed self-diffusion coefficient for D-carnitine in different **D-1** concentration

C° (mM)	D_{obs} (10^{-12} m^2. s^{-1})	χ_{bound}
5	317	0.71
3	320	0.70
1.5	309	0.71
0.375	396	0.58
0.1875	416	0.56
0	800	0

To determine the measurements, the diffusion coefficients of trimethylammonium group was followed. All measurements were done in D_2O at 300 K.
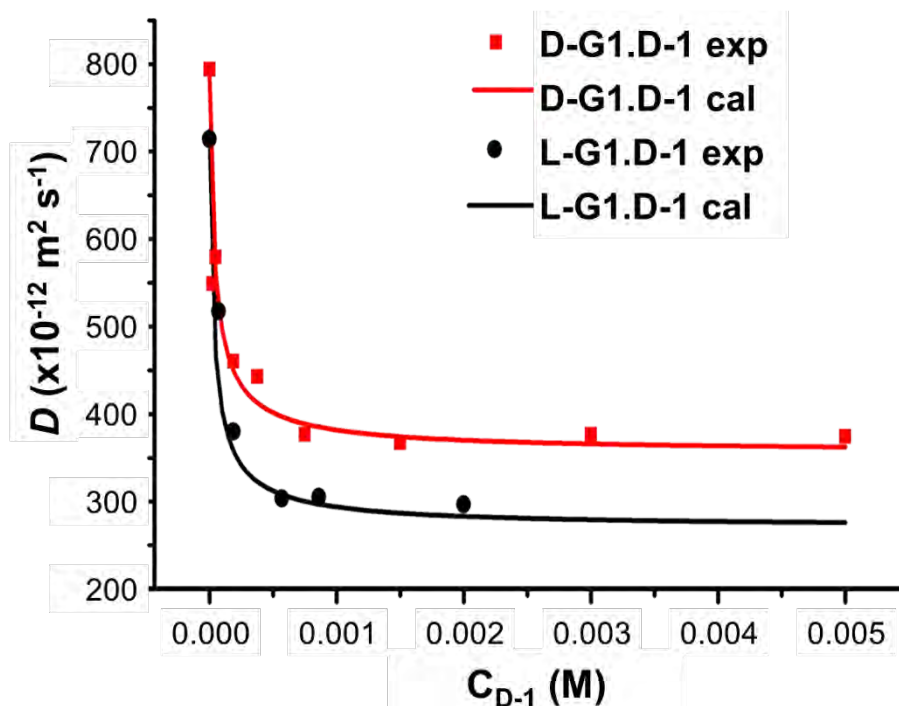

Figure S13. Variation of self-diffusion coefficients of NMe_3^+ for L-G1 and D-G1 in presence of **D-1** (black circles and red squares correspond to experimental data and black and red line correspond to calculated diffusion coefficients).

Table S5. Association constant for L-carnitine and D-carnitine with **D-1**.

Association constant (M^{-1})		Selectivity
$K_{L-G1.D-1}$	$K_{D-G1.D-1}$	K_L/K_D
1250 ± 0.25	1000 ± 0.12	1.25

Encapsulation within the cavity – determination of association constants

Experimental procedure: 50 mg of **L-1** was dissolved in 0.6 ml D_2O. Guests were added to the mixture in excess (around 300 equivalents). The obtained samples were heated at 70 ℃ overnight and allowed to equilibrate at room temperature for one hour. The ^1H NMR spectra reported were obtained directly from these samples.
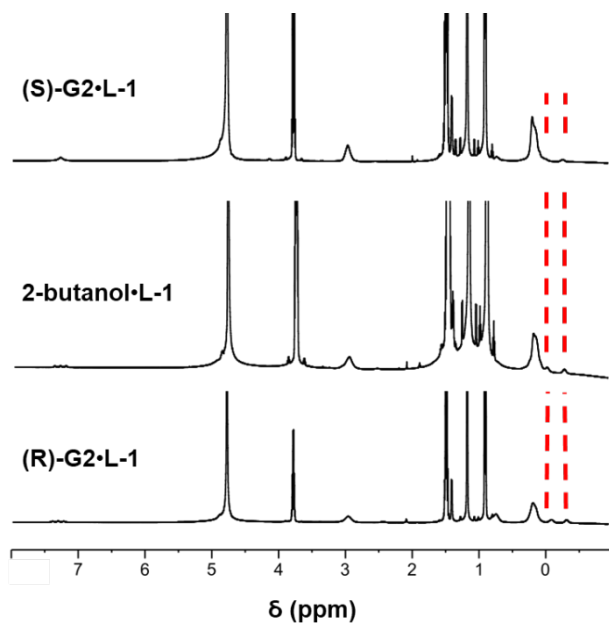
Figure S14. ^1H NMR of **L-1** with racemic, *R*-, and *S*-2-butanol (600 MHz, 300 K). The shifted broad peaks of the encapsulated guest species, used for integration to determine the association constants, are highlighted by the dashed red lines.

The slow exchange, on the NMR timescale, of the added butanol guests between the encapsulated state in the internal cavity and the solvated state, allows for straightforward determination of the association constants using the integration of the free and encapsulated peaks.

6. Crystallography data for L-1

Table S6. Crystal structure and refinement data for **L-1**

Identification code	L-1 (CCDC-1898694)
Empirical formula	C105 H955 Mo132 N49 O773 S
Formula weight	27974.26
Temperature	150(2) K
Wavelength	0.71073 Å
Crystal system	Trigonal
Space group	R -3 :H
Unit cell dimensions	a = 32.669(3) Å $\alpha= 90°$.
	b = 32.669(3) Å $\beta= 90°$.
	c = 73.347(4) Å $\gamma = 120°$.
Volume	67793(11) $Å^3$
Z	3
Density (calculated)	2.056 Mg/m^3
Absorption coefficient	1.878 mm^{-1}
F(000)	41016
Crystal size	0.100 x 0.100 x 0.100 mm^3
Theta range for data collection	1.925 to 25.999°.
Index ranges	-40<=h<=40, -40<=k<=40, -90<=l<=90
Reflections collected	499094
Independent reflections	29610 [R(int) = 0.0401]
Completeness to theta = 25.242°	99.9 %
Absorption correction	Empirical
Max. and min. transmission	0.746 and 0.645
Refinement method	Full-matrix least-squares on F^2
Data / restraints / parameters	29610 / 134 / 1444
Goodness-of-fit on F^2	1.190
Final R indices [I>2sigma(I)]	R1 = 0.0521, wR2 = 0.1365
R indices (all data)	R1 = 0.0608, wR2 = 0.1537
Extinction coefficient	n/a
Largest diff. peak and hole	2.34 and -1.15 e.$Å^{-3}$

7. References

[1] A. Mueller, E. Krickemeyer, H. Boegge, M. Schmidtmann, and F. Peters. *Angew. Chem. Int. Ed.* **1998**, *37,* 3360–3363.

[2] A. Mueller, E. Krickemeyer, H. Boegge, M. Schmidtmann, B. Botar, and M. O. Talismanova. *Angew. Chem. Int. Ed.* **2003**, *42*, 2085–2090.

[3] G. Sheldrick, *ActaCrystallographica Section A*, **1990**, *46*, 467-473.

[4] G. Sheldrick, *ActaCrystallographica Section A*, **2008**, *64*, 112-122.